

铝合金超声搅拌复合焊接

贺地求, 李 剑, 李东辉, 梁健章

(中南大学 高性能复杂制造国家重点实验室, 长沙 410083)

摘 要: 铝合金的搅拌摩擦焊(FSW)通常在焊接区形成上高下低“浅漏斗状”的温度场,使焊缝厚度方向的组织性能差异较大。为了得到更好的焊接效果,文中提出超声搅拌复合焊思想,将超声波通过搅拌头导入焊缝纵深处,以改善焊缝组织性能。试验采用2.5 mm厚的2219铝合金分别用上述两种方法进行焊接,并对焊缝的微观组织和力学性能进行了分析比较。结果表明,两种方法焊接的2219铝合金均可得到成形美观内部无缺陷的焊缝,超声搅拌复合焊的焊缝力学性能明显要优于搅拌摩擦焊。

关键词: 超声搅拌复合焊; 搅拌摩擦焊; 2219 铝合金

中图分类号: TG453 文献标识码: A 文章编号: 0253-360X(2011)12-0070-03



贺地求

0 序 言

目前,搅拌摩擦焊技术已经取得了巨大的进步,在航空、航天、高速舰船、高速铁路列车等工业领域得到广泛的应用^[1,2]。随着研究的深入,焊接过程中反复出现的一些问题也引起了人们的关注。厚板的焊接中由于搅拌摩擦焊上高下低的生热机制容易引起焊缝底部温度不够,导致底部材料流动不充分,出现弱焊、疏松,影响焊缝强度^[3]。薄板的焊接中因为温度差异会引起变形、残余应力大、底部虚焊等缺陷。上高下低的温度场是搅拌摩擦焊所固有的特点,这对焊接过程中材料流动组织均匀化起到了一定的负面影响。针对搅拌摩擦焊在铝合金焊接方面存在的局限性,为了有效的解决焊接过程中焊缝底部温度偏低等问题,文中提出超声搅拌复合焊技术。

1 超声搅拌复合焊接原理

超声波用于生产中主要有4种常见的基本效应:声空化效应、声流效应、热效应、机械效应^[4]。超声塑性加工的优点主要是能够大幅降低变形力,降低流动应力,因此也被广泛应用于超声振动拉伸、薄板深拉深成形、超声挤压、塑料超声焊接等方面^[5-7]。

文中提出的超声搅拌复合焊基本思路是在搅拌摩擦焊中加入超声能,将搅拌针和超声的换能器变

幅杆连为一体,这样搅拌针会附加有超声频振动,如图1所示。超声搅拌焊接技术将超声振动的能量导入到焊缝深层,能够降低焊接流变的抵抗力,减小残余应力,以达到改善焊缝组织,提高焊缝强度的目的,同时超声的加入还可以起到细化晶粒、改善金属宏观和微观偏析的效果^[8,9]。

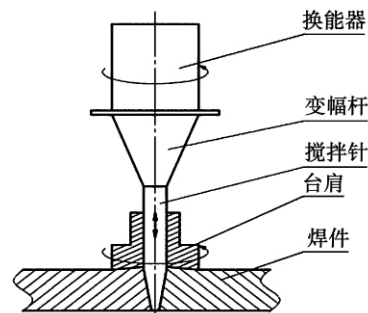


图1 超声波加工系统原理图

Fig. 1 Processing theory of ultrasonic stir compound welding

2 超声搅拌复合焊接试验

2.1 试验的目的及方案

试验的主要目的是验证超声搅拌复合焊技术能否在焊接过程中对2219铝合金的焊接产生积极效果。试验的方案是在各项工艺参数一致的前提下,对同一种材料(2219铝合金)进行超声搅拌焊和搅拌摩擦焊不同的焊接技术来进行对比试验,并通过

尝试不同的焊接参数来找出超声搅拌复合焊对 2219 铝合金的最佳焊接效果.

2.2 试验材料

焊接试验用材料为 2.5 mm 厚的 2219 T87 铝合金轧制板, 焊接尺寸规格为 300 mm × 150 mm (两块). 焊接方式为单道对接焊. 2219 铝合金的化学成分和力学性能见表 1.

表 1 2219 铝合金主要化学成分(质量分数, %) 和力学性能
Table 1 Chemical compositions and mechanical property of 2219 aluminum alloy

Cu	Mn	Ti	Zr	Fe	Al	抗拉强度 R_m /MPa	断后伸长率 A (%)
6.38	0.32	0.064	0.18	0.18	>92	450	11

2.3 试验设备及过程

试验中超声搅拌的换能器为夹心式压电陶瓷, 加装自行设计的工作频率为 20 kHz 的超声振动系统, 组成超声搅拌焊试验系统. 试验用搅拌头参数是: 轴肩直径 6 mm; 搅棒针直径 2.5 mm, 搅拌针长 2.2 mm.

2.4 试验结果分析

焊接试样力学拉伸试验数据如表 2 ~ 表 4 所示.

表 2 搅拌摩擦焊试样力学拉伸试验数据

Table 2 Mechanics stretch test data of FSW specimens

截面尺寸 $a \times b / (mm \times mm)$	拉应力 σ_m / kN	抗拉强度 R_m / MPa	断后伸长率 A (%)	
Y11	14.90 × 2.30	10.982	332.350	10.0
Y12	14.90 × 2.30	11.113	333.286	10.0
Y13	14.90 × 2.30	11.542	336.790	10.8
平均值	—	—	334.142	—

表 3 超声搅拌复合焊力学拉伸试验数据

Table 3 Mechanics stretch test data of ultrasonic stir compound welding specimens

截面尺寸 $a \times b / (mm \times mm)$	拉应力 σ_m / kN	抗拉强度 R_m / MPa	断后伸长率 A (%)	
Y21	14.90 × 2.30	12.18	355.530	9.5
Y22	14.90 × 2.30	12.014	353.450	9.5
Y23	14.90 × 2.30	11.895	350.250	9.0
平均值	—	—	353.077	—

表 2 和表 3 的焊接工艺参数为 2 000 r/min, 进给速度为 20 × 3.56 mm/min, 其中, 表 2 为搅拌摩擦焊, 在此参数条件下 2219 铝合金的搅拌摩擦焊接

表 4 最佳参数超声搅拌焊试样拉伸试验数据表

Table 4 Mechanics stretch experiment data of ultrasonic stir compound welding specimens with most appropriate weld parameters

截面尺寸 $a \times b / (mm \times mm)$	拉应力 σ_m / kN	抗拉强度 R_m / MPa	断后伸长率 A (%)	
Y31	14.90 × 2.30	13.443	392.260	11.0
Y32	14.90 × 2.30	13.471	393.110	10.5
Y33	14.90 × 2.30	13.419	391.840	10.0
平均值	—	—	392.403	—

能够达到最好的焊接效果, 表 3 为其同等条件下的超声搅拌复合焊接对比试验数据. 表 4 的焊接工艺参数为 1 000 r/min, 进给速度为 30 × 3.56 mm/min, 在此工艺参数下超声搅拌复合焊对 2219 铝合金的焊接能够达到最理想的效果. 超声频率锁定在 20.5 kHz 左右, 电压 400 V 左右, 这个参数范围内超声振动能够得到最佳效果. 从拉伸试验报告数据可以看出, 超声搅拌复合焊的抗拉强度比搅拌摩擦焊的强度明显要高, 不同的焊接工艺参数, 所得到的抗拉强度不同, 但是强度的提高是明显的. 在最佳参数下超声搅拌焊接的焊接效果可以达到母材的 87.22%. 这说明超声已经成功引入到焊接过程, 和搅拌摩擦焊相结合并产生了积极的效应, 在一定程度上减少了变形阻力和流动应力.

2.5 显微硬度分析

取焊缝横截面中部的硬度分布, 曲线如图 2 所示. 图中 0 点为焊缝中心位置, 硬度值大体呈“W”型分布, 说明在焊接过程中焊缝各阶层出现了不同程度的软化. 热影响区和热力影响区整体硬度平均约为 85 HV, 最低硬度为 73 HV, 主要出现在热影响区和热力影响区的过渡区, 说明这个区域是焊缝的薄弱之处. 整体硬度差比较明显, 结合金相图来看, 说明显微硬度的变化与微观组织及温度变化紧密相

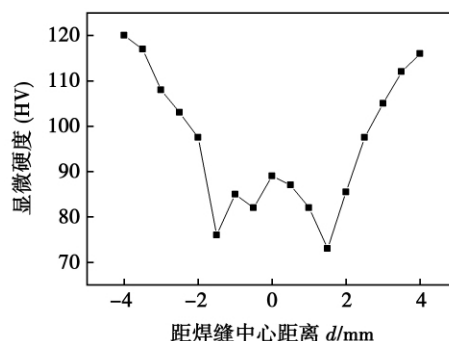


图 2 2219 超声搅拌复合焊焊缝显微硬度分布

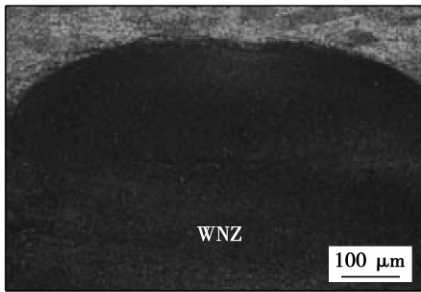
Fig. 2 Microhardness of ultrasonic stir compound welding of 2219 welds

关. 而焊缝处各测试点硬度值相对较高,说明超声的导入有细化晶粒,改善温度影响的积极效果.

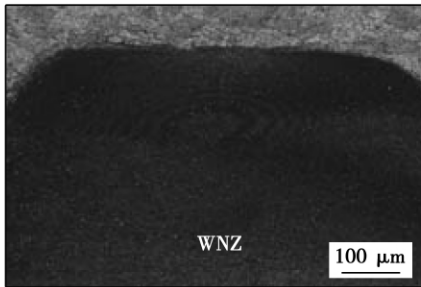
2.6 焊缝显微金相图对比分析

2.6.1 焊核区金相对比

图3为2219焊缝焊核区(weld nugget zone, WNZ)金相对比图. 从整体上来看两者的晶粒都非常细小,这是由于这部分组织受到搅拌头强烈的搅拌作用以及剧烈摩擦产生的局部高温作用,造成大量晶粒破碎,破碎的晶粒发生动态再结晶. 图3b的“洋葱环”比图3a更为明显,结构间距比较大,材料流动更为流畅,这说明超声在细化晶粒减小流变阻力方面有着一定的积极效果.



(a) FSW焊核区



(b) 超声搅拌复合焊焊核区

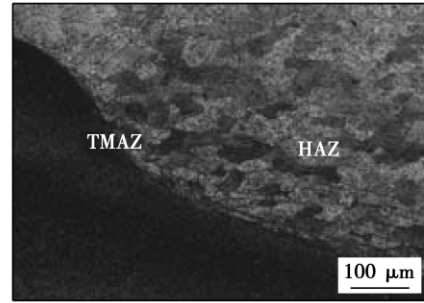
图3 焊核区金相图对比

Fig. 3 Compared nugget zones

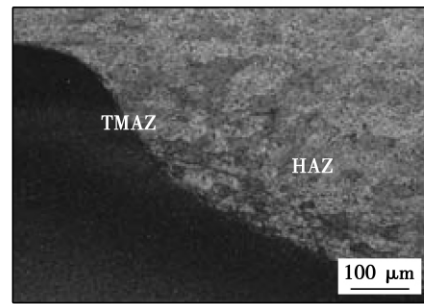
2.6.2 热力影响区和热影响区

图4为焊缝热力影响区(thermal mechanical affected zone, TMAZ)和热影响区(heat-affected zone, HAZ)的显微组织. 热力影响区材料强烈搅拌作用下,其原始的板条状组织发生了较大的弯曲变形和破碎,并在局部范围内发生回复和晶粒长大,与焊核区相比,其晶粒尺寸较为粗大. 热影响区没有受到搅拌作用,但由于焊接中温度热的影响,导致该区域的原始组织略有长大. 从图4显微组织来看,超声搅拌复合焊的热影响区和热力影响区明显要小于搅拌摩擦焊,超声的振动使得在温度偏低的情况下材料也可以有很好的流动,同时焊缝晶粒较为细小且

分布相对比较均匀,热影响区和焊核区分界非常明显,说明超声的振动可提高金属塑性流动,改善焊缝组织.



(a) FSW热力影响区和热影响区



(b) 超声搅拌复合焊热力影响区和热影响区

图4 热力影响区和热影响区金相组织对比

Fig. 4 Comparison of microstructures in thermo-mechanically affected zone and heat affected zone

2.6.3 焊缝整体金相图对比

图5为两种焊缝金相组织整体对比. 从图5中看出,超声搅拌复合焊金相组织晶粒较为细小,热影响区和热力影响区的区域范围比搅拌摩擦焊金相图明显缩小,而且在前进边与热影响区之间形成较大的弯曲边界,而搅拌摩擦焊的晶粒就相对显得比较



(a) FSW金相整体形貌



(b) 超声搅拌复合焊金相整体形貌

图5 焊缝显微金相整体对比

Fig. 5 Comparison of microstructures in plate joint overall

- 业出版社, 2005.
- [2] 张嗣伟. 我国摩擦学工业应用的节约潜力巨大[J]. 中国表面工程, 2008, 21(2): 50-52.
Zhang Siwei. Enormous economy potential of tribology application in industry in china [J]. China Surface Engineering, 2008, 21(2): 50-52.
- [3] Tjong S C, Ma Z Y. Microstructure and mechanical characteristics of in situ metal matrix composites [J]. Materials Science and Engineering, 2000, 29: 49-113.
- [4] Maity Y P C, Panigrahi S C. Metal and intermetallic matrix in situ particle composites [J]. Key Engineering Materials, 1995, 108/110: 313-328.
- [5] Srivatsan T S. Tensile deformation and fracture behavior of a titanium-alloy metal-matrix composite [J]. Composites Part A, 1997, 28A: 365-376.
- [6] 肖代红, 黄伯云. 原位合成钛基复合材料的最新进展 [J]. 粉末冶金技术, 2008, 26(3): 217-223.
Xiao Daihong, Huang Boyun. New progress on in situ titanium matrix composites [J]. Powder Metallurgy Technology, 2008, 26(3): 217-223.
- [7] 宋思利. 钨极氩弧原位合成 TiC 增强铁基熔敷层的研究 [D]. 山东大学, 2007.
- [8] 王振廷, 陈丽丽, 张显友. 钛合金表面氩弧熔覆 TiC 增强复合涂层组织与性能分析 [J]. 焊接学报, 2008, 29(9): 43-45.
Wang Zhenting, Chen Lili, Zhang Xianyou. Microstructure and properties of TiC reinforced composite coating fabricated on Ti alloy by GTAW [J]. Transactions of the China Welding Institution, 2008, 29(9): 43-45.

作者简介: 王振廷, 男, 1965 年出生, 博士后, 教授. 主要从事耐磨材料和材料表面工程方面的教学和科研工作. 发表论文 40 余篇. Email: wangzt2002@163.com

[上接第 72 页]

粗大 热影响区范围比较大. 金相的变化说明超声振动的能量成功地注入到焊缝的底部, 金属组织有较为明显的晶粒细化和组织均匀化的积极效果, 加入超声振动能有效地改善金属的塑性流动状态, 改善焊缝效果.

3 结 论

(1) 提出了超声搅拌复合焊的新方法, 在对 2219 铝合金的试验中尝试将超声波通过搅拌针导入焊缝底部, 以减少变形阻力和流动应力, 提高焊缝底部材料的流动性能, 获得高质量焊缝.

(2) 2219 铝合金超声搅拌焊接试验效果非常明显, 超声的导入使得晶粒更加细小, 组织分布更均匀, 材料的流动性有很明显的改善.

(3) 超声搅拌焊得到的铝合金焊缝抗拉强度大大提高, 显微组织更致密更均匀, 证实了超声搅拌复合焊接能够对铝合金焊接过程产生积极改善效果, 用超声搅拌复合焊接改善材料焊缝底部组织的思路是可行的.

参考文献:

- [1] 张 华, 林三宝, 吴 林, 等. 搅拌摩擦焊研究进展及前景展望 [J]. 焊接学报, 2003, 24(3): 91-96.
Zhang Hua, Lin Sanbao, Wu Lin. *et al.* Progress and prospects of friction stir welding [J]. Transactions of the China Welding Institution, 2003, 24(3): 91-96.
- [2] 周鹏展, 钟 掘, 贺地求, 等. 2519 厚板搅拌摩擦焊接工艺组织分析 [J]. 中南大学学报, 2006, 37(4): 114-118.
Zhou Pengzhan, Zhong Jue, He Diqu. *et al.* Organization analysis of 2519 thick plate friction stir welding process [J]. Centre South University Journal, 2006, 37(4): 114-118.
- [3] 周鹏展, 李东辉, 贺地求, 等. 2219-T6 厚板搅拌摩擦焊沿厚度方向的性能差异 [J]. 焊接学报, 2007, 28(10): 5-8.
Zhou Pengzhan, Li Donghui, He Diqu. *et al.* The performance difference along the thickness direction of 2219-T6 friction stir welding [J]. Transactions of the China Welding Institution, 2007, 28(10): 5-8.
- [4] 金长善. 超声加工 [M]. 哈尔滨: 哈尔滨工业大学出版社, 1989.
- [5] 何 勃, 闻邦春. 振动塑性加工的进展及若干问题 [J]. 辽宁工学院学报, 1999, 19(4): 8-10.
He Qiong, Wen Bangchun. Progress and many issues of vibrations plastic processing [J]. Journal of Liaoning Institute, 1999, 19(4): 8-10.
- [6] Yang S Q, Dang Z, Yah J C, *et al.* Simulation on heating process in ultrasonic welding of plastics [J]. Acta Metallurgica Sinica, 2000, 13(1): 80-83.
- [7] Devine J. Ultrasonic plastics welding basics [J]. Welding Journal, 2001, 80(3): 29-33.
- [8] Eskin G I. Ultrasonic treatment of light alloy melts [M]. Amsterdam: Gordon & Breach, 1998.
- [9] Abramov O V. Action of high intensity ultrasonic on solidifying metal [J]. Ultrasonic, 1987, 25(2): 73-82.

作者简介: 贺地求, 男, 1963 年出生, 硕士, 教授. 主要从事厚板搅拌摩擦焊接工艺及机理研究. 发表论文 20 余篇. Email: wc3lijian@126.com

Through comparing the simulation results and experimental measurements , the prediction accuracy of the developed thermo-elastic-plastic FEM based on Quick Welder was verified. Meanwhile , the influence of welding sequence on the residual stress distribution was clarified using numerical simulation method. The results show that both transverse residual stress and longitudinal residual stress were significantly affected by deposition sequence. The deposition sequence not only largely changes the peak values of residual stress , but also alters the shape of residual stress distribution.

Key words: numerical simulation; non-linear analysis; welding residual stress; welding sequence

Nanoindentation measurement of Sn-Cu-Ni joint WANG Jianxin , LAI Zhongmin , SUN Dandan (Province Key Lab of Advanced Welding Technology , Jiangsu University of Science and Technology , Zhenjiang 212003 , China) . p 59 - 62

Abstract: In order to study the effect of intermetallic compound on mechanical properties of joint , the elastic modulus and hardness of intermetallic compounds were analyzed by nanoindentation method , and the creep strain rate sensitivity of solder matrix was obtained by Mayo-Nix method. From the physical analysis of nanoindentation curves , the elastic modulus of (Cu , Ni)₆Sn₅ in Sn-Cu-Ni joints is 113.2 GPa ± 4.8 GPa , while the hardness is 5.59 GPa ± 0.32 GPa. It is found that intermetallic compounds are the key factors in the reliability of lead-free joints , due to the big contrasts between mechanical properties of intermetallic compounds and solder matrix. The creep strain rate sensitivities of Sn-Cu-Ni , Sn-Cu-Ni-0.05Ce and Sn-Pb solder matrix are 0.1286 , 0.1248 , and 0.1832 , and the creep stress exponents are 7.7760 , 8.0128 , and 5.4585 , respectively , which indicate the improvement in creep resistance of Sn-Cu-Ni joints due to Ce addition.

Key words: lead-free solder; nanoindentation; elastic modulus; creep strain rate sensitivity

Interfacial microstructure of sintering composites of PCBN grains-graphite particles-CuSnTi alloy ZHANG Bin , DING Wenfeng , XU Jiuhua , CHEN Zhenzhen , SU Honghua , FU Yucan (College of Mechanical and Electrical Engineering , Nanjing University of Aeronautics and Astronautics , Nanjing 210016 , China) . p 63 - 65 , 69

Abstract: Sintering experiments of Cu-Sn-Ti alloy , polycrystalline cubic boron nitride (PCBN) abrasive grains and graphite particles were carried out at the heating temperature of 920 °C with the dwell time of 30 min. The strength of sintering bulks was measured by means of the three-point bending experiments. The interfacial microstructure and the phases of the sintering bulks were characterized using scanning electron microscope (SEM) , energy dispersion spectrometer (EDS) and X-ray diffraction (XRD) . The results reveal that in the case of the graphite content of 5 ~ 15 wt% , the bending strength of the composite bulks is above 91 MPa , which is much higher than that of the bulk strength of the vitrified grinding wheels. The elemental diffusion behavior has taken place across the joining interface between PCBN grains and Cu-Sn-Ti alloy in the sintering process. The compounds were formed , therefore , the PCBN grains were bonded firmly. Under such condition , the breakage of the PCBN grains has played the most important role in the fracture of the composite bulks. In particular , the breakage mode of the PCBN

grains is the intergranular fracture.

Key words: PCBN abrasive grains; Cu-Sn-Ti alloy; bending strength; interfacial microstructure

Finite element analysis of temperature field during keyhole-plasma arc welding using SYSWELD software HU

Qingxian¹ , WANG Yanhui¹ , YAO Qingjun² , WANG Shun Yao¹ (1. Provincial Key Lab of Advanced Welding Technology , Jiangsu University of Science and Technology , Zhenjiang 212003 , China; 2. Jiangsu Province Special Equipment Safety Supervision Inspection Institute , Yangzhou Branch , Yangzhou 225003 , China) . p 66 - 69

Abstract: Considering the weld geometric characters of keyhole plasma arc welding (K-PAW) , a suitable and adaptive combined heat source for numerical simulation is developed , i. e. at the transverse cross-section and along the workpiece thickness direction , the double-ellipsoidal volumetric heat source acts at upper part of the workpiece while a linearly-increased peak value of heat flux in gaussian cylinder mode exerts at lower part of the workpiece. Based on the developed adaptive combined heat source model , the welding temperature field of 6 mm thickness stainless steel is simulated by SYSWELD. The predicted weld geometry and fusion line locus at cross-section are in good agreement with the experimental measurement. This demonstrates the suitability of the combined volumetric heat source mode.

Key words: keyhole plasma arc welding; temperature field; combined volumetric heat source; finite element analysis

Study on ultrasonic stir hybrid welding of aluminum alloy

HE Diqiu , LI Jian , LI Donghui , LIANG Jianzhang (State Key Laboratory of High-performance Complex Manufacturing , Central South University , Changsha 410083 , China) . p 70 - 72 , 108

Abstract: Friction stir welding (FSW) of aluminum alloy usually results in a special "funnel shaped" temperature field , which makes obvious difference of microstructure properties in the direction of weld seams. In order to get better properties of welded joints , ultrasonic stir hybrid welding technology has been put forward in this paper , which concentrates the ultrasonic energy in deep weld seams through the stirring pin. Thickness of 2.5 mm 2219 aluminum alloy sheets has been adopted and welded by the two technologies mentioned above in this experiment , microstructure and mechanical properties of weld are analyzed and compared as well. Result shows that the weld joints of 2219 aluminum welded by the two technologies are both with good appearance and defect-free in the inner , and ultrasonic stir hybrid welding obviously has better mechanical properties.

Key words: ultrasonic stir hybrid welding; friction stir welding; 2219 aluminum alloy

Effect of Nd addition on microstructure and mechanical property of Sn3.8Ag0.7Cu solder joint GAO Lili , XUE

Songbai , WANG Bo (College of Materials Science and Technology , Nanjing University of Aeronautics and Astronautics , Nanjing 210016 , China) . p 73 - 76

Abstract: The effects of Nd addition(0 , 0.05 , 0.5wt%) on the microstructure and shear strength of SAC solder joint under as-reflowed and 150 °C isothermal-aging process were investigated. Experimental results showed that Nd addition can obviously improve the shear strength and microstructure of the SAC solder joints. The growth rate of the SAC/Cu interfacial layer as